Biomolecules & Biomedicine

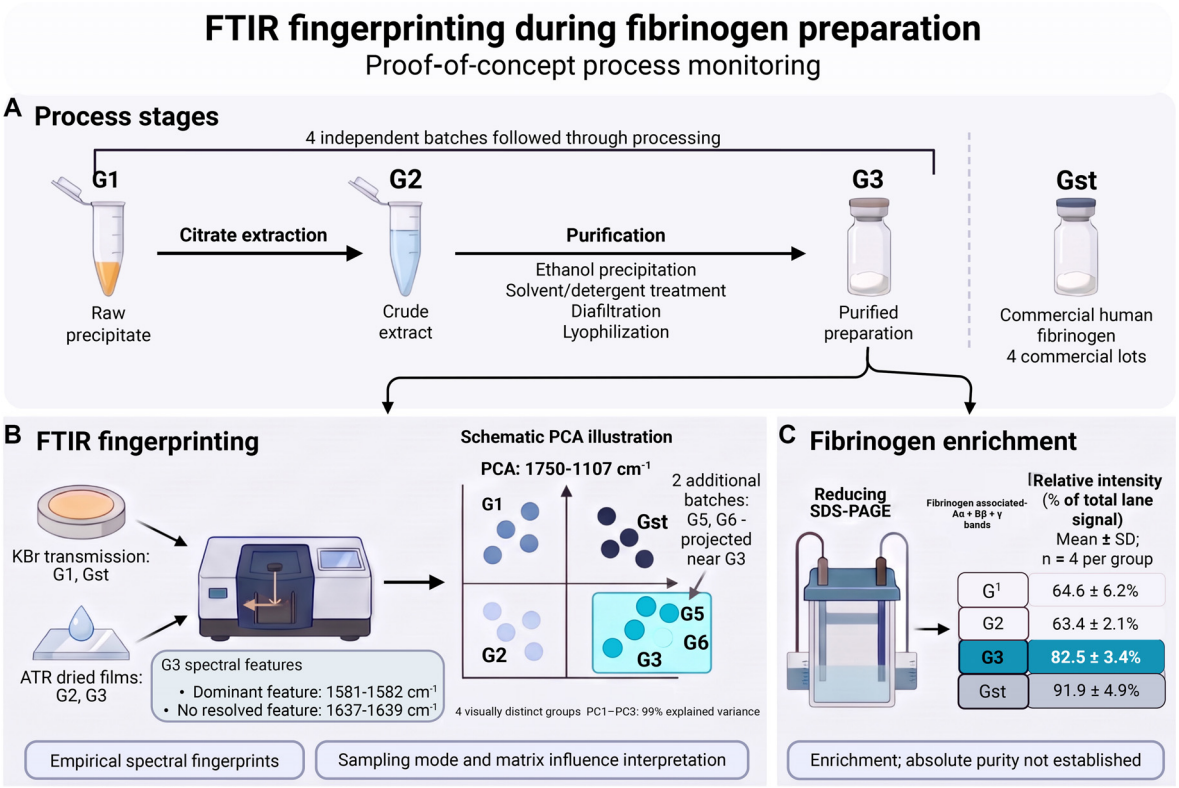
RESEARCH ARTICLE

FTIR spectroscopy and chemometrics for monitoring fibrinogen-containing preparations during purification

Nikolay A. Ryabov, Olga A. Karyakina, Anastasiia A. Surkova, Denis G. Alekseev*, Elena V. Kudinova, Alisa A. Klyuchnikova, Larisa T. Volova

*Correspondence to Denis G. Alekseev: sashsas63@gmail.com

Graphical Abstract



Created in BioRender. Skenderi, E. (2026) https://BioRender.com/hjcruj7

Highlights

- FTIR–PCA reveals four distinct clusters across process and comparator materials.
- Two additional batches project near the purified-preparation cluster.
- Relative fibrinogen-associated gel-band intensity rises from 64.6% to 82.5%.
- Spectral fingerprints do not establish absolute purity or protein structure.

In brief

Ryabov et al. combine Fourier transform infrared spectroscopy with principal component analysis to monitor the purification of fibrinogen-containing preparations in biotechnological production. Spectral patterns separate sample groups, while SDS-PAGE supports fibrinogen enrichment. These empirical fingerprints show promise for process monitoring, but sampling mode and matrix influence interpretation. Harmonized sampling and external validation are required before routine implementation.

DOI: 10.17305/bb.2026.14830

Biomolecules & Biomedicine

RESEARCH ARTICLE

FTIR spectroscopy and chemometrics for monitoring fibrinogen-containing preparations during purification

Nikolay A. Ryabov[1], Olga A. Karyakina[1], Anastasiia A. Surkova[2], Denis G. Alekseev[1*], Elena V. Kudinova[1,3], Alisa A. Klyuchnikova[3], and Larisa T. Volova[1]

Batch-to-batch variability in fibrinogen-containing plasma fractionation by-products complicates standardization, necessitating rapid process-monitoring tools. This proof-of-concept study explored Fourier transform infrared (FTIR) spectroscopy combined with principal component analysis (PCA) to monitor a fibrinogen-containing preparation during processing. We analyzed raw precipitate, crude extract, and purified preparation from four independent production batches, alongside four commercial human fibrinogen lots, using FTIR spectroscopy and reducing sodium dodecyl sulfate–polyacrylamide gel electrophoresis (SDS-PAGE). PCA of spectra in the 1750–1107 cm^{-1} region revealed four visually distinct clusters, with the first three principal components accounting for 99% of the total variance. Two additional final-product batches projected near the purified-preparation cluster. The purified preparation lacked a resolved feature at 1637–1639 cm^{-1} and exhibited a dominant band at 1581–1582 cm^{-1}. SDS-PAGE demonstrated that the combined relative intensity of fibrinogen-associated Aα, Bβ, and γ bands increased from 64.6 ± 6.2% in raw precipitate to 82.5 ± 3.4% after purification, indicating fibrinogen enrichment rather than absolute purity. Due to differences in sampling configuration and matrix, spectral interpretation was limited to empirical fingerprints rather than direct measures of purity, aggregation, or secondary structure. These preliminary findings support further development of FTIR spectroscopy with PCA for process fingerprinting. However, routine implementation requires harmonized sampling, a larger number of independent production batches, predefined acceptance criteria, and external validation.

Keywords: Fibrinogen, plasma fractionation by-products, Fourier transform infrared spectroscopy, chemometrics, principal component analysis, in-process control, quality control.

Introduction

Each year, over 20 million liters of donor plasma are processed globally to produce plasma-derived therapeutics like albumin, immunoglobulins, and coagulation factors [1]. The multi-step Cohn ethanol fractionation process yields these therapeutic proteins along with significant quantities of side fractions, which are often discarded [2]. Fibrinogen-containing precipitate (FP) is one such by-product, commonly treated as process waste. However, recent reconsideration has identified plasma-fractionation by-products as potential sources of biologically active materials when appropriately processed [1]. Fibrinogen- and fibrin-based materials are biocompatible and promote cell adhesion and migration, making them promising candidates for tissue engineering and regenerative medicine [3, 4]. FP also contains co-occurring plasma proteins, including fibronectin, albumin, immunoglobulins, and complement proteins, which can influence the final preparation's biological properties. For instance, fibronectin's arginine-glycine-aspartic acid (RGD) motif supports cell adhesion, while albumin performs transport and antioxidant functions [5, 6].

However, FP composition varies across plasma pools and process conditions, hindering standardization and potential biomedical applications. Protein-composition methods like liquid chromatography–tandem mass spectrometry (LC–MS/MS) offer detailed molecular information but are time-consuming, require specialized equipment and expertise, and may be impractical for routine in-process testing at manufacturing sites [7].

We previously developed a method to produce a fibrinogen-containing preparation from precipitate I, a by-product of donor-plasma fractionation [8]. Process monitoring and final-product standardization necessitate a rapid method to assess batch consistency and detect significant changes in composition or protein conformation.

Fourier transform infrared (FTIR) spectroscopy can detect changes in protein conformation and aggregation. Vibrational

[1]Samara State Medical University, Samara, Russia; [2]Laboratory for Hybrid Nanostructures for Biomedicine, ITMO University, St. Petersburg, Russia; [3]State Budgetary Healthcare Institution, Samara Regional Clinical Blood Transfusion Center, Samara, Russia.

*Correspondence to Denis G. Alekseev: sashsas63@gmail.com

DOI: 10.17305/bb.2026.14830

© 2026 Ryabov et al. This article is available under a Creative Commons License (Attribution 4.0 International, as described at https://creativecommons.org/licenses/by/4.0/).

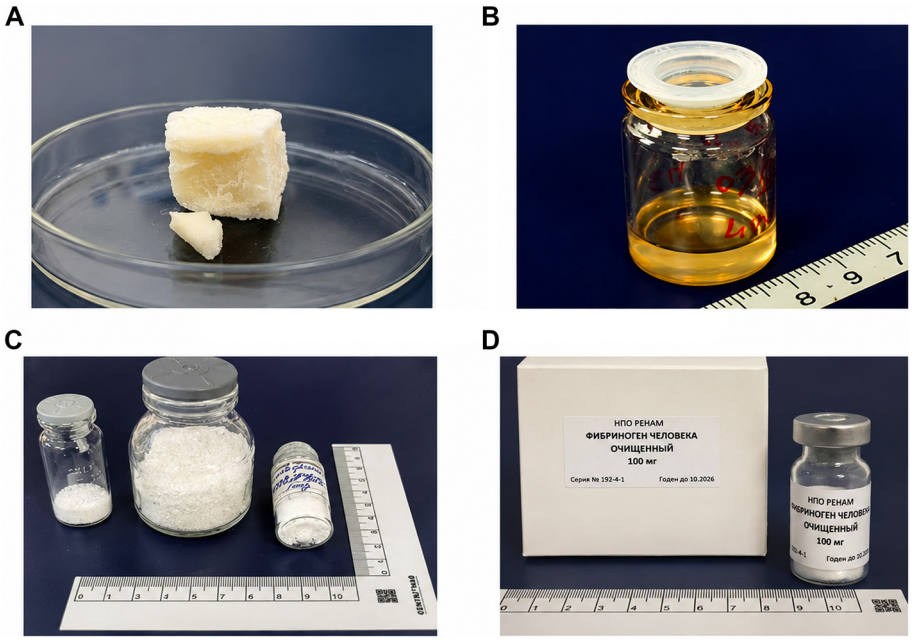


Figure 1. Representative fibrinogen-containing materials at successive processing stages and the commercial comparator. (A) G1, the raw semisolid precipitate collected during donor-plasma fractionation. (B) G2, the crude aqueous extract obtained by extracting G1 with citrate buffer. (C) G3, the purified preparation in lyophilized form. (D) Gst, commercial lyophilized human fibrinogen used as an external comparator. Rulers are shown for size reference. **Abbreviations**: G1, raw fibrinogen-containing precipitate; G2, crude fibrinogen-containing precipitate extract; G3, purified fibrinogen-containing preparation; Gst, commercial human fibrinogen comparator.

spectroscopy, combined with chemometric analysis, has been applied to assess the quality of biopharmaceutical products [7, 9–11]. Machine learning-assisted FTIR microspectroscopy can identify proteins in dry films within minutes, detect differences between purification batches (due to post-translational modifications or conformations), and assess glycosylation [12]. In protein analysis, the amide I, II, and III regions provide complementary information, though band positions and intensities are also affected by hydration, excipients, amino acid side chains, sample preparation, and measurement configuration [13]. Similarly, Raman spectroscopy, combined with principal component analysis (PCA), has been used to differentiate monoclonal-antibody preparations subjected to thermal, oxidative, or concentration-related stress [10]. When proteins aggregate, spectra show intense bands at 1620–1630 cm^{-1}, corresponding to intermolecular β-sheets, making this spectral range an aggregation marker [14, 15]. To date, FTIR-based chemometric monitoring has not been systematically evaluated for fibrinogen-rich side fractions from plasma processing.

This proof-of-concept study aimed to evaluate an FTIR spectroscopy–PCA workflow for rapid, exploratory monitoring of a fibrinogen-containing preparation during processing. We also sought to compare spectral findings with reducing sodium dodecyl sulfate–polyacrylamide gel electrophoresis (SDS-PAGE) profiles.

Given that FTIR spectra were acquired under different measurement modes (potassium bromide [KBr] pellets vs. attenuated total reflectance [ATR]), spectral differences between groups are interpreted as empirical fingerprints of the process stage and measurement conditions, rather than standalone indicators of secondary structure or protein integrity.

Materials and methods

The study workflow involved: (1) forming four sample groups representing different process stages or comparator material; (2) acquiring FTIR spectra; (3) orthogonal characterization by reducing SDS-PAGE; (4) exploratory PCA; and (5) qualitatively comparing spectral features with gel band-intensity profiles.

Samples

Four sample groups were studied (Figure 1): fibrinogen-containing precipitate (G1), crude fibrinogen-containing precipitate extract (G2), purified fibrinogen-containing preparation (G3), and commercial human fibrinogen (Gst). G1–G3 materials were lyophilized using an AK2-55 freeze dryer (Lyogen, Russian Federation) with the following cycle: freezing at −45 °C for 12 h, primary drying at −10 °C and 0.2 mbar for 24 h, and secondary drying at 25 °C and 0.1 mbar for 12 h.

For attenuated total reflectance–Fourier transform infrared spectroscopy (ATR-FTIR) measurements of liquid samples, lyophilized material was reconstituted in 10 mM citrate buffer (pH 7.8) to a protein concentration of 3–5 mg/mL. For SDS-PAGE, lyophilized material was reconstituted in sample buffer as described below.

G1 (raw FP)

This wet, semi-solid starting material was collected from the donor-plasma fractionation process at the Samara Regional Clinical Blood Transfusion Center without additional purification. Aliquots were lyophilized before FTIR transmission measurements in KBr pellets and before SDS-PAGE. G1 represented the process starting material.

G2

Five grams of wet precipitate from each G1 batch were mixed with 10 mM citrate buffer using a laboratory homogenizer (Witeg, Germany) at low speed for 3–4 min at a precipitate-to-buffer ratio of 1:10 (w/v). The suspension was incubated for 30 min at room temperature and centrifuged at 10,000 × g for 5 min at 4 °C. The supernatant was retained, and the pellet was rehomogenized with an additional volume of citrate buffer corresponding to a 1:5 precipitate-to-buffer ratio (w/v), followed by a second centrifugation under the same conditions. The two supernatants were combined. G2 represented the crude aqueous extract used for subsequent purification.

G3

G3 was prepared from G2 according to the method described in [8]. Briefly, absolute ethanol pre-cooled to −20 °C was added to the combined G2 supernatant with continuous stirring at 300 rpm to achieve a final ethanol (substance-liquid 95%; RFK, Russia) concentration of 8% (v/v). The mixture was incubated at 0 ± 1 °C for 18 h to precipitate the fibrinogen-containing fraction. The precipitate was collected by centrifugation at 3,000 × *g* for 10 min at 4 °C and dissolved in 10 mM citrate buffer (pH 7.8) at a precipitate-to-buffer ratio of 1:50 (w/v).

For solvent/detergent treatment to inactivate enveloped viruses, tri-n-butyl phosphate (TnBP) (Merck, Germany) and Triton X-100 (Pallav, India) were each added to a final concentration of 1% (v/v). The mixture was incubated at 30 ± 2 °C for 4 h with stirring at 100 rpm. Low-molecular-weight process residuals, including detergent and ethanol, were removed by diafiltration against 10 mM citrate buffer (pH 7.4) using a tangential-flow filtration (TFF) system (BIO-RUS LLC, Russia) equipped with a 10-kDa molecular-weight-cutoff polysulfone membrane (Cobetter, China). The diafiltration buffer volume was at least five times the sample volume, and the transmembrane pressure was 0.5 bar. The retentate was concentrated to the initial G2 volume.

The quantitative verification of process residual removal (TnBP, Triton X-100, and ethanol) was not performed in this proof-of-concept study; this represents a limitation that will be addressed in future work.

The solution was lyophilized using the cycle described above. Product yield was calculated as the dry mass of lyophilized G3 divided by the dry mass of the corresponding G1 precipitate and expressed as a percentage. Figure 2 summarizes the preparation process.

Gst

Lyophilized human fibrinogen (batch 1924/1-1924/4; 100 mg/vial; RPA RENAM, Russian Federation) served as an external comparator. According to the manufacturer, the formulation contains buffer components, process-related additives, and stabilizers; these constituents were treated as formulation excipients rather than protein impurities. The material was reconstituted in deionized water at 3–5 mg/mL. Gst was not considered a certified reference material or an equivalence standard.

G1, G2, and G3 were obtained longitudinally from four independent 600-L donor-plasma pools collected on different days, yielding four independent process batches. Gst was analyzed using four vials from different commercial lots. Thus, each group comprised four independent batch- or lot-level samples ($n = 4$ per group).

For a preliminary assessment of process repeatability, two additional independent final-product batches (G5 and G6) were prepared from newly collected raw material using the G3 procedure. These batches were not used to fit the PCA model and were not analyzed by SDS-PAGE.

FTIR spectroscopy

FTIR spectra were acquired from 4000 to 500 cm^{-1} using an FT-801 FTIR spectrometer (SIMEX LLC, Russian Federation).

The sampling configuration was selected based on the physical properties of each material (Figure 3) [16]. Lyophilized G1 and Gst were sufficiently friable to be ground with KBr and measured in transmission mode as KBr pellets. Additionally, G1's incomplete solubility would form a turbid suspension unsuitable for homogeneous ATR film formation, while Gst contains formulation excipients that could concentrate during drying, distorting the spectrum. These factors further supported KBr transmission for G1 and Gst. Lyophilized G2 and G3 formed fibrous, elastic masses that could not be reproducibly pulverized; KBr pellets from these materials were opaque, heterogeneous, and produced substantial scattering. Therefore, G2, G3, G5, and G6 were analyzed as dried films using ATR. Because the measurement configuration was linked to the sample group, between-group comparisons were interpreted as empirical spectral fingerprints rather than unambiguous differences in protein secondary structure. All subsequent spectral comparisons are treated as exploratory fingerprinting, with no causal assignment to protein conformation or purity made without orthogonal evidence.

Lyophilized G1 and Gst were ground with spectroscopic-grade KBr (TR 6-09-3946-87, Russian Federation) at an approximate sample-to-KBr mass ratio of 1:100 and pressed into pellets at 150–200 bar. Spectra were collected from 4000–500 cm^{-1} at a spectral resolution of 8 cm^{-1} by co-adding 100 scans. A pure KBr pellet served as the background spectrum. Measurements were performed at a relative humidity below 30% to minimize water uptake.

Aliquots of 2–3 μL of G2, G3, G5, and G6 were placed on the diamond ATR crystal and air-dried at 20 ± 5 °C until a visually homogeneous protein film formed, typically within 15–20 min. Drying minimized bulk-water absorbance. Spectra were acquired over the same range (4000–500 cm^{-1}), at 8 cm^{-1} resolution, with 100 co-added scans. A clean ATR crystal was used to collect the background spectrum.

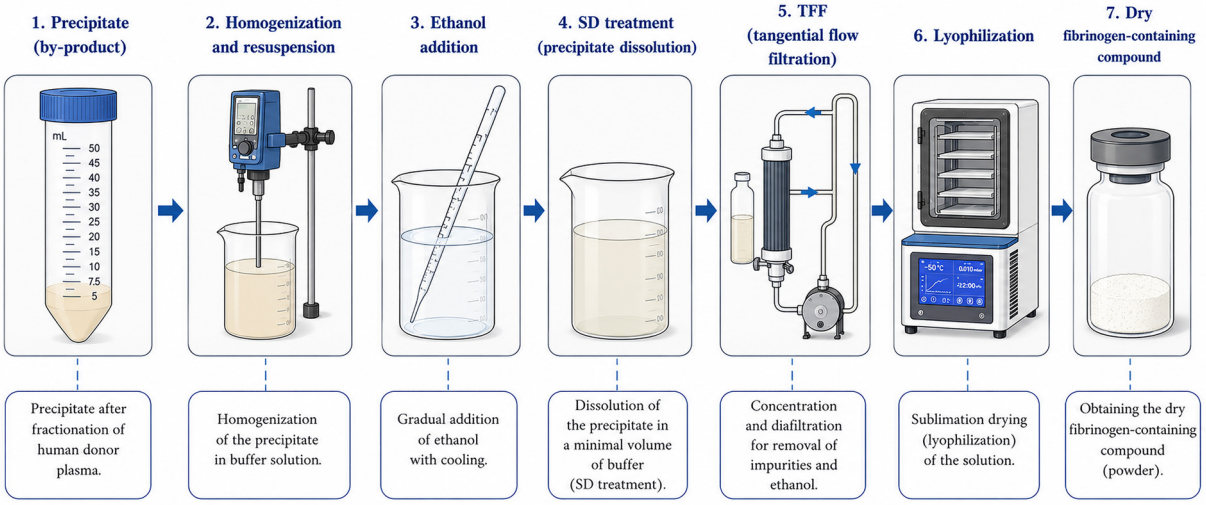


Figure 2. Production workflow for a lyophilized fibrinogen-containing preparation from a donor-plasma fractionation by-product. (1) Collection of the raw precipitate (G1). (2) Homogenisation and extraction in citrate buffer to obtain the crude extract (G2). (3) Gradual addition of pre-cooled ethanol to precipitate the fibrinogen-containing fraction. (4) Recovery and dissolution of the precipitate in citrate buffer, followed by SD treatment with tri-n-butyl phosphate and Triton X-100. (5) Diafiltration and concentration using TFF, intended to reduce low-molecular-weight process residuals, including ethanol and detergent. (6) Lyophilisation of the concentrated solution. (7) Recovery of the dry fibrinogen-containing preparation (G3). Removal of process residuals was not quantitatively verified in this study. **Abbreviations**: G1, raw fibrinogen-containing precipitate; G2, crude fibrinogen-containing precipitate extract; G3, purified fibrinogen-containing preparation; SD, solvent/detergent; TFF, tangential-flow filtration.



Figure 3. FT-801 FTIR spectrometer and sampling accessories. The instrument is shown with an ATR accessory installed in the sample compartment and a separate solid-sample holder in the foreground. The ATR accessory was used to analyse dried protein films, whereas the solid-sample holder was used for transmission measurements of samples prepared as KBr pellets.**Abbreviations**: ATR, attenuated total reflectance; FTIR, Fourier transform infrared; KBr, potassium bromide.

The effective ATR penetration depth, which is wavelength- and matrix-dependent, was expected to be on the order of 1–2 micrometers.

Between measurements, the ATR crystal and pellet-die surfaces were cleaned sequentially with 70% ethanol and deionized water. A blank spectrum was then collected to verify the absence of residual protein bands.

Reducing SDS-PAGE

Lyophilized G1, G2, G3, and Gst materials from the same four batches or lots used for FTIR spectroscopy were analyzed by reducing SDS-PAGE ($n = 4$ independent samples per group).

Electrophoresis was performed according to the Laemmli method using a 15% polyacrylamide resolving gel [17].

Gels were run in a vertical WIX-easy PRO4 Mini chamber (Wix Technology Co. Ltd., China) with 7 × 8 cm glass plates. A 10–250 kDa prestained molecular-mass marker (Bio-Rad, USA) and reference proteins at 25, 50, and 75 kDa were used. Marker proteins were not heat-treated, and 7 μL of marker stock was loaded per lane.

5 mg of each lyophilized sample was solubilized in 2.5 mL of sample buffer containing 62.5 mM Tris(hydroxymethyl)aminomethane hydrochloride (Tris-HCl) (pH 7.2) (NPP PanEco LLC, Russia), 4 M urea (analytical grade;

Obolensk, Russia), and 2% sodium dodecyl sulfate (Central Drug House (P) Ltd., India). β-Mercaptoethanol (Merck, Germany) was added to 5% (v/v), and samples were heated in boiling water for 5 min. Bromophenol blue (CAS 115-39-9; NPP PanEco LLC, Russia) was added to a final concentration of 0.04%, and 10 μL of sample solution was loaded per lane. Electrophoresis was performed at 120 V until proteins entered the resolving gel, then at 180 V for approximately 1 h. Gels were stained with Coomassie Brilliant Blue G-250 (VWR International, USA), destained twice in 10% ethanol containing 8.5% acetic acid, and then washed in 7% acetic acid for 2–3 days. Gel images were quantified using Image Lab software, version 6.1.0 build 7 (Bio-Rad, USA).

One lane was analyzed for each independent sample, yielding four sample lanes per group.

Ethical statement

The study was approved by the Bioethics Committee of Samara State Medical University (meeting minutes No. 312, November 25, 2025).

Statistical analysis and chemometrics

Relative SDS-PAGE band-intensity data were analyzed by one-way analysis of variance (ANOVA) followed by Tukey's multiple-comparisons test for comparisons among G1, G2, G3, and Gst. Distributional assumptions were assessed using the Shapiro–Wilk test, and homogeneity of variance was assessed using Levene's test. All tests were two-sided, and $P < 0.05$ was considered statistically significant. Because each group contained only four independent samples, inferential results were interpreted as exploratory. Analyses were performed in GraphPad Prism, version 9.5 (GraphPad Software, USA).

PCA was performed in The Unscrambler X, version 9.7 (Camo Analytics, Norway), to explore major sources of spectral variation, reduce dimensionality, and visualize similarities among samples [18]. To avoid inflating the influence of technical replicates, the three replicate spectra of each independent sample were first averaged to obtain one spectrum per batch or lot. For samples acquired in ATR mode (G2, G3, G5, and G6), the averaged spectra were subjected to the built-in diamond ATR correction. All batch- or lot-averaged spectra were then restricted to the 1750–1107 cm^{-1} region, preprocessed using Standard Normal Variate (SNV), and mean-centered before PCA. Each of the four groups used to construct the PCA model (G1, G2, G3, and Gst) was represented by four independent batch- or lot-level spectra. G5 and G6 were subsequently projected onto the fitted model and were not used for model construction. Scores plots were used to visualize sample distributions, and loading plots were examined to identify spectral regions associated with separation.

Results

A lyophilized fibrinogen-containing preparation (G3) was obtained from each G1 batch using the procedure described above. Mean product yield, calculated as dry G3 mass relative to dry G1 mass, was 65 ± 5% (mean ± standard deviation [SD]; $n = 4$ independent batches). The product formed a porous white cake that readily dissolved in citrate buffer to yield a clear solution without visible particles.

FTIR spectroscopy

Characteristic FTIR bands

All band positions and intensities reported below are empirical; they reflect the combined influence of protein composition, conformation, excipients, physical state, and measurement mode, and should not be overinterpreted as direct structural or purity indicators.

Figure 4A shows the mean unprocessed FTIR absorbance spectra. The strongest group-discriminating variation occurred in the 1750–1000 cm^{-1} region, which includes the amide I, II, and III bands. Amide I (approximately 1700–1600 cm^{-1}) arises predominantly from peptide C=O stretching; amide II (approximately 1600–1500 cm^{-1}) primarily reflects N–H bending coupled with C–N stretching; and amide III (approximately 1300–1200 cm^{-1}) contains mixed C–N stretching and N–H bending contributions (Figure 4B) [7, 19].

Major and additional bands observed for each sample group are summarized in Table 1. Batch-level statistics for selected band positions are presented in Table 2.

G2 displayed a prominent feature at 1637–1639 cm^{-1}, a region that can contain contributions from β-sheet-rich protein structures. G3 lacked a resolved amide I maximum and showed only weak shoulders at 1657–1659 cm^{-1}. The dominant feature at 1581–1582 cm^{-1} was therefore treated as an empirical marker of this process stage rather than as a conventional amide II band. Gst showed a strong feature at 1613–1615 cm^{-1} and multiple additional bands. Because Gst contained formulation excipients and was measured in KBr transmission mode, these bands cannot be assigned solely to protein conformation.

Across groups, the batch-level SD of selected peak positions did not exceed 2 cm^{-1}. Reported coefficient of variation (CV) values ranged from 0.02% to 0.13%. For doublet bands, each component was summarized separately. Because CV is strongly influenced by the large absolute wavenumber value, the SD in cm^{-1} provides a more direct estimate of peak-position repeatability.

Exploratory PCA of process-stage and commercial materials

PCA was performed on averaged, ATR-corrected, and SNV-preprocessed spectra within the 1750–1107 cm^{-1} region, following mean-centering. This analysis aimed to identify spectral regions responsible for sample separation using scores and loadings plots. The first three principal components (PC1, PC2, and PC3) collectively explained 99% of the total variance: PC1 accounted for 64%, PC2 for 27%, and PC3 for 8%.

Figure 5 displays the scores plots for PC1/PC2 and PC2/PC3, alongside their corresponding loading vectors for PC1–PC3. In the PC1/PC2 scores plot, spectra formed four visually distinct clusters corresponding to G1, G2, G3, and Gst. PC1 separated G1 (negative scores) from G3 (positive scores), with G2 and Gst positioned in intermediate regions. Strong contributions to PC1 were observed from spectral regions near 1657, 1638, 1582, and 1529 cm^{-1}. PC2 primarily differentiated G1 (negative scores) from G2 (positive scores), while G3 and Gst clustered around

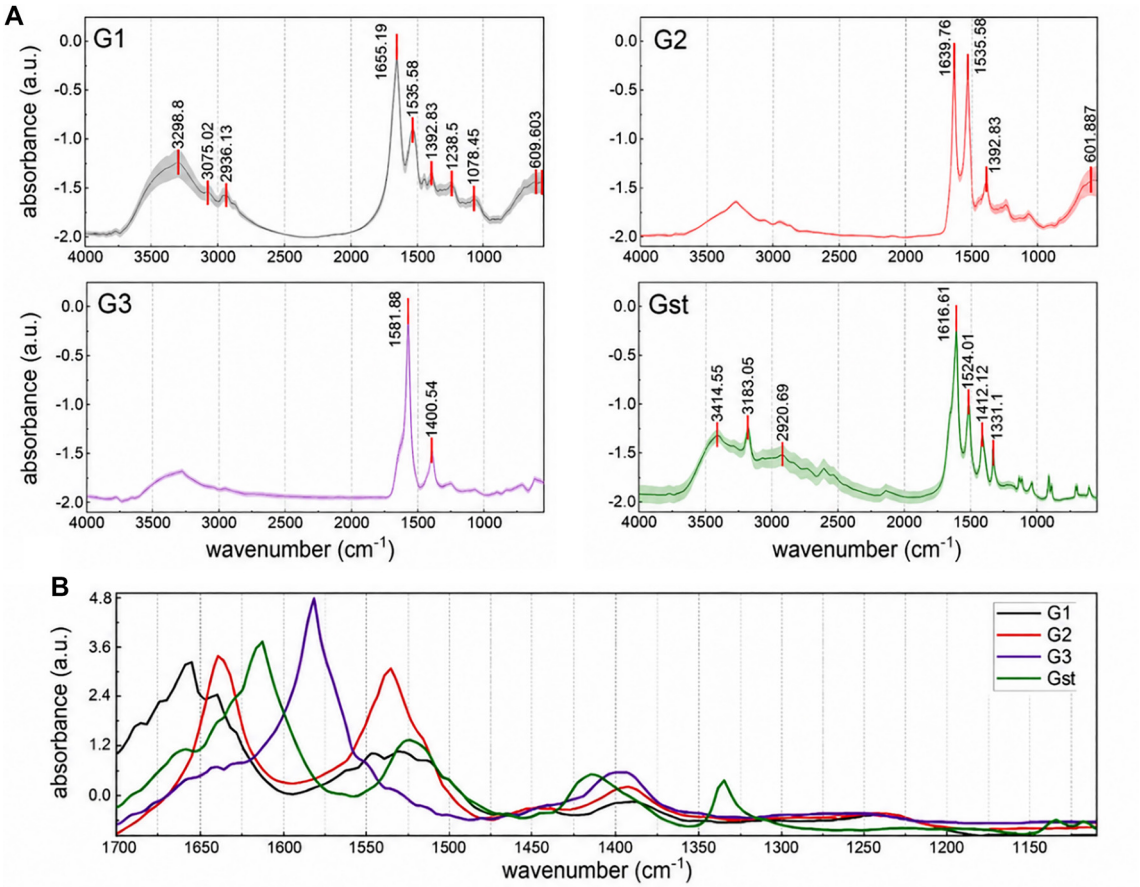


Figure 4. FTIR spectral fingerprints of fibrinogen-containing materials across processing stages and the commercial comparator. (A) Mean unprocessed absorbance spectra over 4000–500 cm^{-1}; solid lines represent means and shaded areas indicate SD. Selected peak positions are labelled in cm^{-1}. (B) Overlaid SNV-preprocessed spectra highlighting group-specific profiles in the amide I, II and III regions. Colors denote G1 (black), G2 (red), G3 (purple) and Gst (green). Four independent batches or lots were analyzed per group, with three technical spectra acquired per sample.G1 and Gst were measured in transmission mode as KBr pellets, whereas G2 and G3 were analyzed as dried films by ATR. Differences in sampling mode, matrix and formulation limit interpretation to empirical spectral fingerprints rather than direct measures of protein purity, aggregation or secondary structure. **Abbreviations**: ATR, attenuated total reflectance; a.u., arbitrary units; FTIR, Fourier transform infrared; G1, raw fibrinogen-containing precipitate; G2, crude fibrinogen-containing precipitate extract; G3, purified fibrinogen-containing preparation; Gst, commercial human fibrinogen comparator; KBr, potassium bromide; SD, standard deviation; SNV, standard normal variate.

Table 1. Major and additional bands observed in FTIR spectra

Group	Amide I region, cm^{-1}	Amide II/overlapping region, cm^{-1}	Amide III region, cm^{-1}	Additional bands, cm^{-1}
G1	1656–1658	1546 and 1530 (doublet)	1236–1239	1395; 1446; 1075–1076
G2	1637–1639	1536–1538	1241–1243	1392; 1453; 1076
G3	No resolved maximum[1]	1581–1582; shoulders at 1657–1659[2]	1252–1256	1395–1400 (doublet); 1078
Gst	1613–1615; shoulder at 1657–1659	1524–1525	1221–1223	1443–1445; 1413–1415; 1335–1337; 1191–1193; 1134–1136; 1116–1118; 1040–1042

[1]No distinct amide I maximum was resolved in G3. [2]Weak shoulders were observed at 1657–1659 cm^{-1}, whereas the dominant feature in the 1700–1500 cm^{-1} region occurred at 1581–1582 cm^{-1}. Because this frequency is higher than the conventional amide II maximum and overlaps with contributions from carboxylate, amino acid side-chains, and buffer, the assignment is considered tentative. **Abbreviations:** FTIR, Fourier transform infrared; G1, raw fibrinogen-containing precipitate; G2, crude fibrinogen-containing precipitate extract; G3, purified fibrinogen-containing preparation; Gst, commercial human fibrinogen comparator.

the center of the PC2 axis. The loadings defining this component were predominantly influenced by bands near 1636, 1582, and 1536 cm^{-1}. Given that the groups were measured using different sampling configurations, these loadings may reflect a combination of compositional variations, conformational changes, excipient presence, physical states, and measurement modes.

Table 2. Batch-level summary of selected FTIR band positions (mean ± SD and CV; $n = 4$ independent batches)

Group	Parameter	Amide I region, cm^{-1}	Amide II/overlapping region, cm^{-1}	Amide III region, cm^{-1}
G1	Mean ± SD	1657.3 ± 1.8	1545.9 ± 1.0/1530.0 ± 1.1	1237.0 ± 1.2
	CV, %	0.1	0.07/0.07	0.10
G2	Mean ± SD	1638.4 ± 1.0	1537.0 ± 1.8	1242.9 ± 0.9
	CV, %	0.06	0.12	0.08
G3	Mean ± SD	—	1582.3 ± 0.4	1254.8 ± 1.1
	CV, %	—	0.03	0.09
Gst	Mean ± SD	1613.9 ± 2.0	1525.2 ± 0.3	1223.6 ± 0.4
	CV, %	0.13	0.02	0.03

Abbreviations: CV, coefficient of variation; FTIR, Fourier transform infrared; G1, raw fibrinogen-containing precipitate; G2, crude fibrinogen-containing precipitate extract; G3, purified fibrinogen-containing preparation; Gst, commercial human fibrinogen comparator; SD, standard deviation.

PC3 effectively separated Gst from the three process-derived groups. Prominent PC3 loadings (Figure 5C) were observed near 1613, 1574, 1547, 1516, 1416, and 1335 cm^{-1}. These features could originate from formulation excipients, protein conformation, or measurement-mode effects; their precise molecular origin was not independently confirmed. The qualitative similarity between the PC3 loading vector and the Gst spectrum supports an association with the commercial formulation but does not identify the specific contributing compounds.

Table 3 provides tentative assignments for spectral regions exhibiting high loadings. Spectra from two additional batches, G5 and G6, were projected into the existing PCA model. In both the PC1/PC2 and PC2/PC3 scores plots (Figure 5A, B), these spectra were located near the G3 observations. This finding suggests preliminary within-process consistency but does not constitute external validation of a classification model.

Electrophoresis

Reducing SDS-PAGE was employed to compare the apparent fibrinogen-chain pattern and other protein bands across various process stages. Gels were stained with Coomassie Brilliant Blue G-250 and quantified by densitometry using a GelDoc Go imaging system (Bio-Rad, USA).

Samples containing fibrinogen exhibited three major bands with apparent molecular masses consistent with human fibrinogen Aα (56 kDa), and γ (~46 kDa) chains [20]. Additional bands were detected above 200 kDa, between 100 and 150 kDa, and at 10–35 kDa. Without specific protein identification, these regions can only be described as putative aggregates, complexes, fragments, or co-occurring proteins.

G3 displayed the expected three-chain fibrinogen pattern along with residual additional bands (Figure 6), which is consistent with a heterogeneous fibrinogen-containing preparation rather than purified fibrinogen alone [8].

Relative band intensity was calculated as the intensity of an individual band or band region divided by the sum of all band intensities in the corresponding lane. Table 4 reports the apparent molecular masses of the major fibrinogen chains, and Table 5 details the relative band-intensity distributions.

The combined relative intensity of the three fibrinogen-associated bands in G3 was 82.5 ± 3.4% (Table 5), indicating fibrinogen enrichment during purification. The apparent molecular mass of the Aα chain was higher and more variable in G1 and G2 compared to G3 and Gst, whereas the Bβ- and γ-chain estimates were broadly similar across all groups (Table 4).

Additional high- and low-molecular-weight bands

G3 showed a lower relative intensity of bands above 200 kDa than G1 and G2; Gst exhibited the lowest value in this region (7.0 ± 0.6%). Bands at 10–35 kDa were detected in G1 and G2 but were not observed in G3 or Gst under the specified staining and imaging conditions. Non-detection should not be interpreted as absolute absence below the method's detection limit. Densitometric results are summarized in Table 5.

It is important to emphasize that these densitometric values represent relative band intensities and do not constitute absolute purity measurements; co-migrating proteins may contribute to the fibrinogen-chain bands.

One-way ANOVA revealed a significant group effect on the combined relative intensity of the three fibrinogen-chain bands ($F(3,12)=23.55$; $P < 0.001$). Tukey's test indicated higher values for G3 (82.5 ± 3.4%) compared to G1 (64.6 ± 6.2%; $P = 0.0054$) and G2 (63.4 ± 2.1%; $P = 0.0016$). The difference between G3 and Gst (91.9 ± 4.9%) was not statistically significant ($P = 0.1747$); however, a lack of statistical significance does not establish equivalence between the two materials.

The relative intensity of bands above 200 kDa was lower in G3 (11.2 ± 0.8%) than in G1 (22.1 ± 2.6%) and G2 (21.4 ± 1.6%; $P < 0.001$ for both comparisons). No bands at 10–35 kDa were detected in G3 or Gst, whereas this region accounted for 11.8 ± 3.1% of total lane intensity in G1 and 8.0 ± 1.2% in G2 ($P < 0.01$ for G3 vs G1 and G2). The 100–150 kDa region was higher in G2 (7.5 ± 2.5%) than in G1 (1.25 ± 0.2%; $P = 0.033$) and Gst (1.2 ± 0.1%; $P = 0.030$). The identities of proteins or fragments in these regions were not determined.

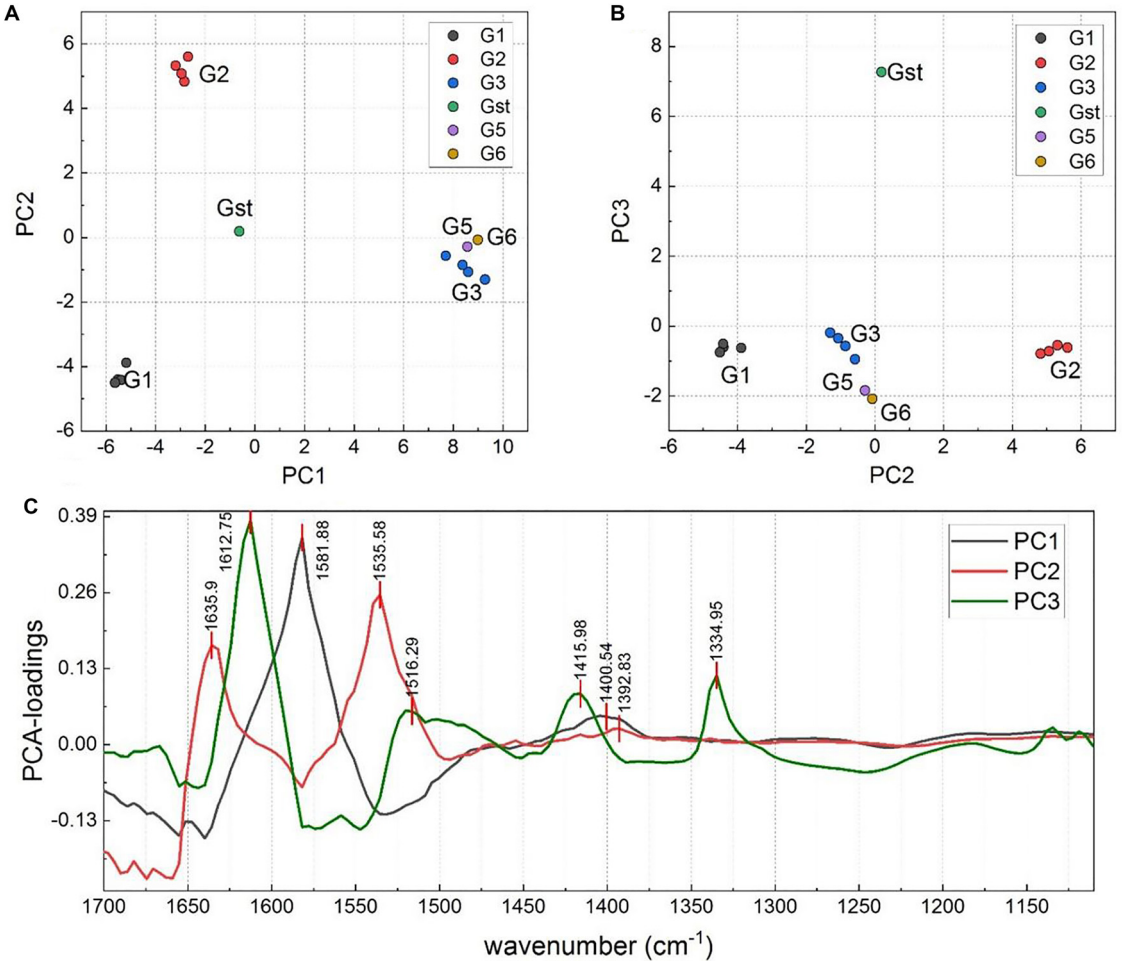


Figure 5. Exploratory PCA of FTIR spectral fingerprints across fibrinogen processing stages and the commercial comparator. (A) PC1–PC2 scores plot. (B) PC2–PC3 scores plot. (C) Loading vectors for PC1 (black), PC2 (red) and PC3 (green), with selected wavenumbers labelled. PC1, PC2 and PC3 explained 64%, 27% and 8% of total variance, respectively. The model was fitted using batch- or lot-averaged spectra from G1, G2, G3 and Gst ($n = 4$ per group), with three technical spectra averaged per independent sample. Spectra were restricted to 1750–1107 cm^{-1} and subjected to ATR correction where applicable, SNV preprocessing and mean-centring. Two additional independent final-product batches, G5 (purple) and G6 (yellow), prepared using the G3 protocol, were projected onto the fitted model without contributing to its construction. Their proximity to G3 provides preliminary evidence of similar spectral fingerprints but does not constitute external validation. Differences in sampling mode and matrix limit interpretation of group separation to exploratory spectral fingerprinting. **Abbreviations**: ATR, attenuated total reflectance; FTIR, Fourier transform infrared; G1, raw fibrinogen-containing precipitate; G2, crude fibrinogen-containing precipitate extract; G3, purified fibrinogen-containing preparation; G5 and G6, additional independent final-product batches prepared using the G3 protocol; Gst, commercial human fibrinogen comparator; PC, principal component; PCA, principal component analysis; SNV, standard normal variate.

Table 3. Tentative assignment of spectral regions with high PCA loadings

PC	Wavenumber, cm^{-1}	Tentative spectral assignment
PC1	1529, 1582, 1638, 1657	1529: amide II; 1582: possible COO^-/side-chain or buffer contribution; 1638 and 1657: amide I region
PC2	1536, 1582, 1636	1536: amide II; 1582: possible COO^-/side-chain or buffer contribution; 1636: amide I/β-sheet-associated region
PC3	1335, 1416, 1516, 1547, 1574, 1613	1335: CH_2/side-chain region; 1416: symmetric stretching of COO^-; 1516 and 1547: amide II; 1574 and 1613: side-chain, COO^-, excipient, and/or amide I contributions

Abbreviations: CH_2, methylene group; COO^-, carboxylate group; PC, principal component; PCA, principal component analysis.

Discussion

SDS-PAGE findings

SDS-PAGE provided orthogonal, albeit nonspecific, evidence of changes in the electrophoretic profile across the purification process.

Under reducing conditions, fibrinogen resolves into Aα, Bβ, and γ polypeptide chains, typically with apparent molecular masses of approximately 63–67, 56, and 47–50 kDa, respectively [20]. Densitometry (Table 4) showed that the combined relative intensity of these chains was approximately

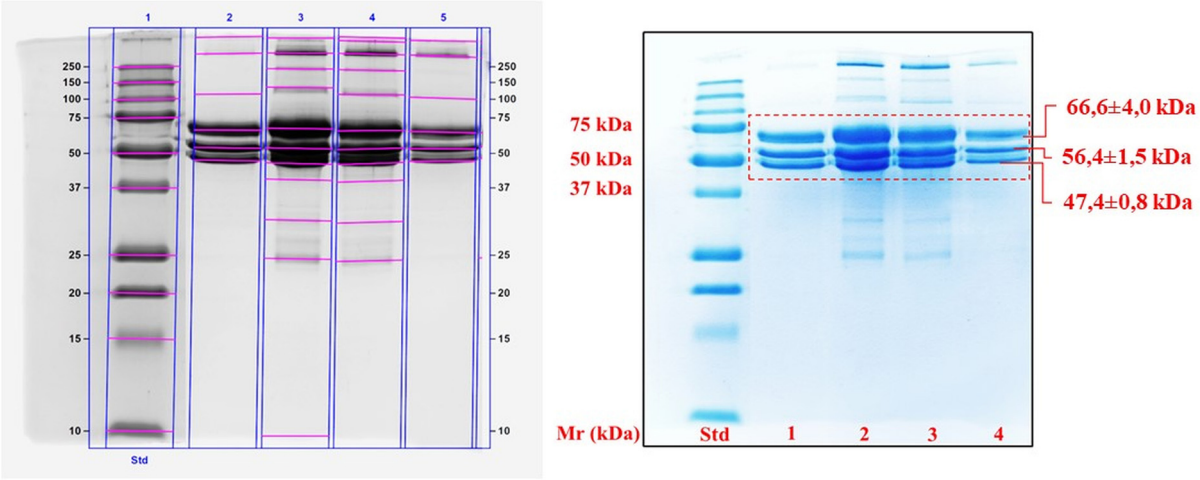


Figure 6. Representative reducing SDS-PAGE profiles of fibrinogen-containing materials across processing stages and the commercial comparator. The same Coomassie Brilliant Blue G-250-stained 15% polyacrylamide gel is shown as an Image Lab screenshot with lane and band annotations (left) and a photograph (right). Lane assignments: Std, 10–250 kDa molecular-mass markers; 1, Gst; 2, G1; 3, G2; and 4, G3. The red dashed box highlights bands with electrophoretic mobilities consistent with the fibrinogen Aα, Bβ and γ chains. The annotated apparent molecular masses refer specifically to G3: 66.6 ± 4.0, 56.4 ± 1.5 and 47.4 ± 0.8 kDa for the Aα, Bβ and γ chains, respectively. These values represent mean ± SD across four independent batches, rather than measurements from the single gel shown. Chain assignments are based on electrophoretic migration and were not independently confirmed by protein identification. **Abbreviations**: G1, raw fibrinogen-containing precipitate; G2, crude fibrinogen-containing precipitate extract; G3, purified fibrinogen-containing preparation; Gst, commercial human fibrinogen comparator; SD, standard deviation; SDS-PAGE, sodium dodecyl sulfate–polyacrylamide gel electrophoresis; Std, molecular-mass standard.

Table 4. Apparent molecular masses of fibrinogen chains estimated by reducing SDS-PAGE across four independent batches

Group	Aα chain apparent molecular mass, kDa (CV, %)	Bβ chain apparent molecular mass, kDa (CV, %)	γ chain apparent molecular mass, kDa (CV, %)
G1	74.7 ± 8.1 (10.8)	54.4 ± 1.9 (3.5)	46.7 ± 1.3 (2.7)
G2	74.3 ± 8.5 (11.4)	54.5 ± 2.5 (4.7)	47.2 ± 1.9 (4.0)
G3	66.6 ± 4.0 (5.9)	56.4 ± 1.5 (2.6)	47.4 ± 0.8 (1.6)
Gst	67.2 ± 2.6 (3.9)	54.8 ± 2.1 (3.9)	48.1 ± 1.5 (3.1)

Abbreviations: CV, coefficient of variation; G1, raw fibrinogen-containing precipitate; G2, crude fibrinogen-containing precipitate extract; G3, purified fibrinogen-containing preparation; Gst, commercial human fibrinogen comparator; SDS-PAGE, sodium dodecyl sulfate–polyacrylamide gel electrophoresis.

Table 5. Relative SDS-PAGE band intensity distributions for test materials

Group	Combined relative intensity of Aα, Bβ, and γ bands, % (CV, %)	Bands >200 kDa, % (CV, %)	Bands at 100–150 kDa, % (CV, %)	Bands at 10–35 kDa, % (CV, %)
G1	64.6 ± 6.2 (9.6)	22.1 ± 2.6 (11.9)	1.25 ± 0.2 (17.0)	11.8 ± 3.1 (26.4)
G2	63.4 ± 2.1 (3.2)	21.4 ± 1.6 (7.6)	7.5 ± 2.5 (33.2)	8.0 ± 1.2 (15.1)
G3	82.5 ± 3.4 (4.1)	11.2 ± 0.8 (6.8)	6.2 ± 0.4 (6.8)	Not detected
Gst	91.9 ± 4.9 (5.3)	7.0 ± 0.6 (8.1)	1.2 ± 0.1 (6.1)	Not detected

Abbreviations: CV, coefficient of variation; G1, raw fibrinogen-containing precipitate; G2, crude fibrinogen-containing precipitate extract; G3, purified fibrinogen-containing preparation; Gst, commercial human fibrinogen comparator; SDS-PAGE, sodium dodecyl sulfate–polyacrylamide gel electrophoresis.

64% in both G1 and G2. In these starting materials, the Aα chain migrated at ~74 kDa, exceeding the typical published range (63–67 kDa) [20, 21]. This shift may be attributed to covalent adducts (e.g., fibronectin cross-linked by factor XIIIa) [22], post-translational modifications such as non-stoichiometric phosphorylation [21] or N-glycosylation [23], or the presence of naturally occurring Aα isoforms (70 and 67 kDa) [24]. However, these possibilities were not experimentally verified in this study and require further confirmation (e.g., by mass spectrometry). After purification (G3), the Aα chain migrated at 66.6 ± 4.0 kDa, consistent with native fibrinogen, suggesting effective removal of modified forms,

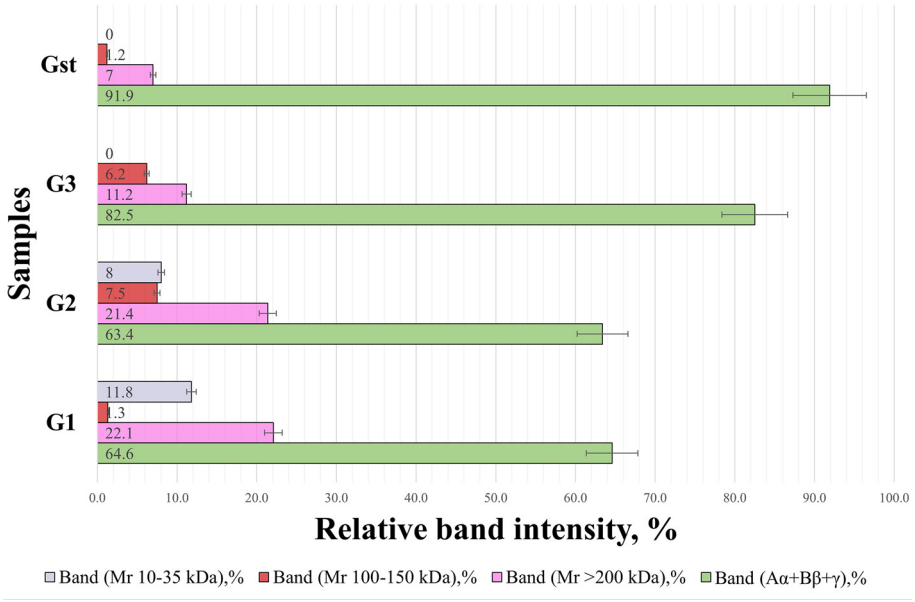


Figure 7. Relative SDS-PAGE band-intensity distributions across fibrinogen processing stages and the commercial comparator. Densitometric analysis of Coomassie-stained reducing SDS-PAGE gels showing the combined relative intensity of fibrinogen-associated Aα, Bβ and γ bands (green) and additional bands at >200 kDa (pink), 100–150 kDa (red) and 10–35 kDa (grey). Intensities were normalized to the sum of all band intensities in the corresponding lane and expressed as percentages. Bars and numerical labels represent means, and error bars indicate SD ($n = 4$ independent batches or commercial lots per group). Bands at 10–35 kDa were not detected in G3 or Gst under the staining and imaging conditions used and are represented as 0%; non-detection does not establish absence below the method's detection limit. These values reflect relative staining intensities rather than absolute protein purity, as co-migrating proteins may contribute to the fibrinogen-associated bands. **Abbreviations**: G1, raw fibrinogen-containing precipitate; G2, crude fibrinogen-containing precipitate extract; G3, purified fibrinogen-containing preparation; Gst, commercial human fibrinogen comparator; SD, standard deviation; SDS-PAGE, sodium dodecyl sulfate–polyacrylamide gel electrophoresis.

aggregates, and proteolytic fragments (the Aα chain is particularly susceptible to proteolysis [20, 25]). The reduced inter-batch variability in the G3 chain estimates indicates more consistent electrophoretic migration, reflecting greater compositional uniformity of the final fibrinogen-containing preparation.

The combined relative intensity of the three chain bands increased to 82.5 ± 3.4% in G3. This result aligns with the expected enrichment of fibrinogen-associated bands after ethanol precipitation and tangential-flow filtration. Nevertheless, Coomassie densitometry provides relative lane intensity rather than absolute protein purity, and proteins that co-migrate with fibrinogen chains may contribute to the measured values. Confirmation of purity will require orthogonal quantitative methods, including LC–MS/MS, size-exclusion high-performance liquid chromatography (SEC-HPLC), immunoblotting, and/or enzyme-linked immunosorbent assay (ELISA), along with a validated fibrinogen activity assay. These analyses are planned for future work. The absence of a statistically significant difference between G3 and Gst should likewise not be interpreted as analytical equivalence. The reduction in bands above 200 kDa and the non-detection of bands at 10–35 kDa support a cleaner electrophoretic profile after processing.

Gst showed the highest combined relative intensity of the three fibrinogen-chain bands (91.9 ± 4.9%; CV 5.3%), consistent with the manufacturer's specifications for this product. However, as SDS-PAGE densitometry is a semi-quantitative method, this result does not independently confirm absolute purity or qualify Gst as a certified reference standard.

Relative intensities in additional gel regions revealed the following patterns:

- **Bands above 200 kDa:** These bands constituted 22.1 ± 2.6% of total lane intensity in G1 and 21.4 ± 1.6% in G2, decreasing to 11.2 ± 0.8% in G3. They may encompass fibrinogen oligomers, cross-linked complexes, incompletely reduced material, or other high-molecular-weight plasma proteins [26]. Their specific identities were not determined. The observed decrease post-purification aligns with the effective removal or reduction of high-molecular-weight species.
- **Bands at 100–150 kDa:** This region represented 1.25 ± 0.2% of total lane intensity in G1, 7.5 ± 2.5% in G2, 6.2 ± 0.4% in G3, and 1.2 ± 0.1% in Gst. The increased content of 100–150 kDa fragments in G2 and G3 might reflect specific characteristics of the sample preparation and purification processes. Fragments around 100 kDa are known to correspond to stable products from restricted fibrinogen hydrolysis, including D and E domains [27]. Notably, these fragments retain their ability to polymerize and, as reported in [27], do not diminish the product's functional activities. The observed increase in the percentage of these fragments in G3 (versus G1) could also be attributed to the efficient removal of other protein impurities (high molecular aggregates and low molecular degradation products), leading to their

relative enrichment in the final product. This hypothesis, however, requires absolute quantification of these fragments (normalized to total protein in the sample), which was not performed in this study. Therefore, this interpretation remains speculative. The commercial material Gst, subjected to more stringent industrial purification, exhibited the lowest content of these fragments.

- **Bands at 10–35 kDa:** This region accounted for 11.8 ± 3.1% of total lane intensity in G1 and 8.0 ± 1.2% in G2, potentially containing proteolytic fragments or other low-molecular-weight proteins [28, 29]. No bands in this range were detected in G3 or Gst under the assay conditions. This finding supports the effective reduction of detectable low-molecular-weight species but does not preclude the presence of material below the staining or densitometric detection limit.

Overall, the purification process yielded a G3 electrophoretic profile characterized by a higher relative contribution from the three primary fibrinogen-chain bands, fewer detectable low-molecular-weight bands, and lower relative intensity above 200 kDa compared to the starting material (Figure 7). While SDS-PAGE serves as a suitable orthogonal batch-comparison assay, definitive assessment of protein identity, absolute purity, and minor components necessitates advanced methods such as LC–MS/MS, immunoblotting, and SEC-HPLC.

Interpretation of FTIR spectral markers

Before drawing any structural or purity-related conclusions, the spectral data must be treated as qualitative fingerprints. The following discussion, therefore, focuses on empirical correlations rather than absolute structural assignments.

The amide I maximum is sensitive to protein secondary structure; α-helix-rich fibrinogen typically displays a feature near 1655–1659 cm^{-1} [7]. In G3, no prominent amide I maximum was resolved; only weak shoulders were observed at 1657–1659 cm^{-1}. Instead, the dominant feature in the 1700–1500 cm^{-1} region occurred at 1581–1582 cm^{-1} [30]. Current publications [31] indicate that approximately 20% of the intensity within 1700–1500 cm^{-1} may originate from amino acid side chains. An amide II peak shift could signify conformational changes leading to more accessible carboxyl groups of aspartic and glutamic acids, thereby producing an intense signal. This aligns with data on the sensitivity of amide II to structural changes [7, 16, 32]. However, the signal could also be partially due to residual citrate buffer. Further studies are required to definitively confirm the nature of this peak.

The 1632–1638 cm^{-1} region can include contributions from β-sheet-rich structures, including intermolecular β-sheets associated with some protein aggregates [12, 15, 33]. However, a feature in this region is not specific to impurities, and its absence does not directly measure protein purity. The absence of absorption in the 1632–1638 cm^{-1} region from the G3 spectrum, a range commonly linked to β-sheet conformations, suggests a preparation with fewer β-sheet-rich structures [12, 33]. While a shift of the amide I band to 1637–1639 cm^{-1} in G2 has been reported as possibly indicating β-structure enrichment from plasma impurities [7], in the present study, this feature might equally be explained by differences in protein composition, conformation, hydration, film morphology, or the measurement configuration, and thus should not be overinterpreted as a direct indicator of impurity content.

Gst exhibited a prominent feature at 1613–1615 cm^{-1}. Although low-frequency amide I bands can be associated with intermolecular β-sheets, this region also overlaps with amino acid side-chain and excipient contributions, and Gst was analyzed using a different sampling configuration than G3 [16, 34]. Therefore, aggregation cannot be inferred solely from this band.

Nevertheless, the 1581–1582 cm^{-1} feature empirically differentiated G3 from G2 and Gst in the current dataset. Until its molecular origin is established, it is more appropriately considered a process-specific fingerprint feature rather than a conventional amide II marker or a direct indicator of purity.

The reduction in additional SDS-PAGE bands in G3 was qualitatively consistent with the distinct G3 FTIR fingerprint. However, no formal correlation analysis was performed, and the FTIR features cannot be assigned to specific gel bands based on the present data.

The batch-level SD of selected FTIR peak positions did not exceed approximately 1.5 cm^{-1}, and CV values ranged from 0.02%–0.13%. These results demonstrate stable peak localization under the study conditions. Given that wavenumber CV values are intrinsically small and the instrument's stated reading accuracy is approximately ±1 cm^{-1}, repeatability should primarily be evaluated using absolute deviations, replicate quality-control samples, and predefined spectral acceptance limits.

Sample preparation and measurement configuration represent major limitations. Compression in KBr may alter or shift protein bands, and ATR spectra of dried films are influenced by film thickness, contact with the crystal, and wavelength-dependent penetration depth [14, 35]. Furthermore, G1 and Gst were measured by KBr transmission, whereas G2 and G3 were measured by ATR. These confounding factors limit direct structural interpretation of between-group differences. A validated in-process method should employ a harmonized sampling configuration throughout the process or develop and validate separate stage-specific models.

In summary, the FTIR features reported here are process-specific empirical markers; they cannot replace orthogonal analytical methods for determining purity, aggregation, or secondary structure.

Interpretation of PCA results

The loading plots identify spectral regions associated with separation in the PCA space but do not establish causal chemical assignments. Features near 1657 and 1638 cm^{-1} fall within the amide I region, while features near 1524–1537 cm^{-1} are consistent with amide II contributions. The 1582 cm^{-1} feature may include carboxylate, side-chain, buffer, or amide contributions. Therefore, PC1 appears to capture a composite of process stage, composition, conformation, and measurement effects rather

than protein purity alone [18]. The 1582 cm^{-1} feature and the PCA separation should be regarded as empirical spectral fingerprints of the process stage rather than definitive structural or compositional markers.

PC2 was associated with features near 1636, 1582, and 1536 cm^{-1} and separated G1 from G2, while G3 and Gst were located near the center of the PC2 axis. Because the groups differ in physical state, formulation, and sampling configuration, this component cannot be attributed specifically to dissolution-induced conformational change or aggregation. The proximity of G3 and Gst along PC2 raises the possibility that the purification process yielded a product with spectral features comparable to those of the commercial reference; however, confirmation would require additional analytical methods.

PC3 separated Gst from the process-derived samples and was associated with features near 1335, 1416, 1516, 1547, 1574, and 1613 cm^{-1}. Formulation excipients and protein conformation [36] may all contribute to these loadings. The qualitative resemblance between the PC3 loading vector and the Gst spectrum supports an association with the commercial formulation, but the responsible chemical species were not identified.

A detailed examination of the citrate contribution was conducted to determine if the observed group separation was influenced by citrate in the formulation. Citrate displays characteristic absorption bands at approximately 1570 and 1392 cm^{-1}. Analysis of the SNV-preprocessed spectra (Figure 4B) revealed higher intensity in the 1392 cm^{-1} region for citrate-containing samples. However, a weak absorption in this region was also present in samples without citrate, suggesting multiple overlapping signals contribute to this spectral window. Crucially, the loadings on all three PCs (Figure 5C) showed only minimal intensity at 1392 cm^{-1}, appearing as very small features rather than prominent peaks. At 1570 cm^{-1}, no corresponding loading features were observed. These findings indicate that citrate is unlikely to be the sole cause of group separation, though contributions from the sample matrix and measurement configuration cannot be ruled out. It is also important to note that samples G2 and G3 were prepared with citrate, while G1 and Gst used KBr. If the preparation method were the primary factor influencing the model, these groups would be expected to form distinct clusters in the score plots. The absence of such clustering further supports the conclusion that the observed separation stems primarily from protein-related differences rather than the sample preparation matrix.

The projection of G5 and G6 near the G3 cluster offers preliminary evidence that the process can generate similar spectral fingerprints in additional batches. However, two projected batches are insufficient to demonstrate model robustness, and PCA is an unsupervised exploratory method, not a validated classifier. Future development should include a larger, prospectively defined set of independent batches, batch-level cross-validation that keeps technical replicates together, external validation from different production campaigns or sites, and predefined acceptance regions and performance criteria.

Performance of the preparation process

The process successfully converted a variable fibrinogen-rich plasma-fractionation byproduct into a more consistent fibrinogen-containing preparation. G1, a wet precipitate from the ethanol-fractionation line, is known for its heterogeneous protein composition, which varies across plasma pools and process campaigns [1, 27].

A two-step citrate extraction yielded G2 with a combined fibrinogen-chain content of approximately 63%. Subsequent ethanol precipitation, solvent/detergent treatment, and tangential-flow filtration increased this value to $82.5 \pm 3.4\%$ in G3, with a mean dry-mass yield of $65 \pm 5\%$ relative to the starting precipitate (G1). These data demonstrate substantial enrichment of fibrinogen-associated bands alongside high material recovery, suggesting a potentially cost-effective route for valorizing a plasma-fractionation byproduct. However, a formal conclusion on economic advantage would require a dedicated process-cost and yield analysis, which was beyond the scope of this proof-of-concept study.

The combined relative intensity of fibrinogen-associated bands in the laboratory G3 preparation ($82.5 \pm 3.4\%$) remained lower than that of the commercial comparator Gst ($91.9 \pm 4.9\%$). This difference is not a shortcoming but a deliberate choice to avoid exhaustive purification steps typically employed for producing highly purified fibrinogen (>90%) via multi-step chromatographic techniques [37, 38]. Instead, the developed protocol intentionally retains a fraction of co-occurring plasma proteins (e.g., fibronectin, albumin, and others) that may contribute to a synergistic biological complex, potentially enhancing the functional performance of the final product in tissue-engineering and regenerative-medicine applications. This approach also offers a cost-effective advantage by utilizing a readily available plasma-fractionation byproduct as the starting material [8]. Nevertheless, the identities, absolute concentrations, functional contributions, batch-to-batch variability, and safety profile of these retained co-proteins remain to be established in future studies; the present data do not demonstrate synergistic activity or equivalence to highly purified fibrinogen products.

SDS-PAGE analysis suggests that the combined purification steps increased the relative fibrinogen-chain signal, reduced bands above 200 kDa, and removed detectable bands at 10–35 kDa. The 100–150 kDa region remained at $6.2 \pm 0.4\%$ in G3, but these bands cannot be assigned to fibrinogen D or E fragments without direct identification. The process therefore appears to balance material recovery with a cleaner electrophoretic profile, while commercial feasibility and product performance remain to be demonstrated.

Practical significance, limitations, and future work

The proposed FTIR spectroscopic approach shows promise as an express in-process control method for producing the fibrinogen-containing compound according to the protocol described in [8]. The observed spectral features, particularly the absence of β-sheet-associated bands in the 1632–1638 cm^{-1} region and the characteristic position of the amide II band

(~1582 cm^{-1}), may serve as rapid empirical markers for assessing product purity and detecting adverse aggregation. However, at present, these features should not be used as standalone measures of purity, secondary structure, or aggregation, as the method has not yet been formally validated. Prior to routine implementation, further validation is required, including harmonized sampling, instrument and operator studies, reference and control materials, predefined acceptance criteria, external validation with an independent set of production batches, and a statistically justified assessment of process repeatability. Importantly, the between-batch variability of the positions of the major spectral bands, expressed as CV, was $\leq$ 0.13% (Table 2), indicating stable peak localization and high reproducibility of the method.

Beyond process monitoring, future studies should establish direct quantitative relationships between the spectral fingerprint and clinically or technologically relevant product attributes. It is well documented that fibrinogen purity profoundly affects the functional properties of fibrin clots. Specifically, the structure and mechanical properties of fibrin gels are closely linked to the fibrinogen heterogeneity profile: monodisperse fibrinogen-derived fibers produce more oriented networks with higher stiffness, whereas polydisperse samples yield weaker, less organized gels [26]. Impurities and degradation products can slow clot polymerization and compromise its mechanical integrity [27], while removal of co-purified proteins such as fibronectin and plasminogen is necessary to obtain reproducible fibrin matrices [39]. Therefore, a particularly promising direction would be a correlative study comparing spectral purity indicators (e.g., amide I/II ratios, absence of β-sheet bands) with functional endpoints such as clotting time, gelation kinetics (turbidimetry), clot ultrastructure, and rheological properties across samples of different purity grades (G1–G3 and Gst). Such an experiment would allow identification of which spectral changes predict compositional and functional integrity rather than merely distinguishing process stages, thereby transforming FTIR from an exploratory fingerprinting tool into a predictive quality-control assay.

The principal limitations are as follows:

- **Limited cross-validation:** For a rigorous assessment of predictive performance, cross-validation should be performed at the batch level, keeping all replicates from the same independent batch together. In this proof-of-concept study, the limited number of independent batches ($n = 4$) prevented batch-level and external validation. Consequently, the model's performance should be considered exploratory. Future work with a larger set of batches from multiple production runs will require batch-level cross-validation and external testing to confirm generalizability.
- **Relative purity measurement:** Coomassie-stained SDS-PAGE densitometry provides relative band intensities, not an absolute measure of protein purity. Proteins co-migrating with fibrinogen chains may contribute to measured values. Therefore, future studies will require orthogonal quantitative methods, including LC–MS/MS, SEC-HPLC, immunoblotting, ELISA, and a validated fibrinogen activity assay, to confirm purity and functional integrity.
- **Lack of formal correlation analysis:** No formal correlation analysis was performed between the PCA spectral components and SDS-PAGE band intensities. Thus, the observed PCA separation may primarily reflect differences in process stage, sample matrix, and measurement configuration rather than a direct quantitative relationship with the electrophoretic protein profile. Further targeted correlation experiments are needed to establish whether specific spectral features predict compositional changes.

Future work

The proposed FTIR-based approach can be adapted for quality control of various plasma-derived protein products, including albumin and immunoglobulins, and for monitoring the storage stability of therapeutic protein formulations. A particularly promising direction is method automation using portable or handheld FTIR spectrometers. This would enable real-time, on-site express analysis directly at blood transfusion centers and manufacturing facilities, eliminating the need for sample transportation to centralized laboratories. However, before such deployment, the method must undergo rigorous validation, including standardization of sampling configuration, incorporation of buffer and excipient blanks, definition and validation of spectral preprocessing protocols, and performance assessment across independent batches from multiple production campaigns or sites. Furthermore, to establish spectral fingerprints as reliable predictors of product quality, future studies should integrate orthogonal quantitative assays such as LC–MS/MS, SEC-HPLC, immunoblotting, and functional clotting tests. Transfer of the method to portable instrumentation should only be considered after successful method-transfer and instrument-comparability studies. Once validated, the approach could serve as both a rapid in-process control tool and a routine stability-monitoring assay, facilitating timely detection of conformational changes or aggregation during storage, thereby enhancing product safety and regulatory compliance.

Conclusion

This proof-of-concept study demonstrated that FTIR spectroscopy combined with PCA could distinguish raw fibrinogen-containing precipitate, its crude extract, the purified preparation, and a commercial comparator, supporting its potential as a rapid fingerprinting tool. However, the approach is not yet validated for routine in-process control. The G3 preparation showed a reproducible empirical fingerprint characterized by the absence of a resolved 1637–1639 cm^{-1} feature and a dominant band at 1581–1582 cm^{-1}. Because sampling mode, matrix, and formulation differed among groups, these features should not yet be interpreted as definitive markers of β-sheet content, aggregation, or protein purity.

Reducing SDS-PAGE supported enrichment of fibrinogen-associated bands: the combined relative intensity of the Aα,

Bβ, and γ bands increased from 64.6 ± 6.2% in G1 and 63.4 ± 2.1% in G2 to 82.5 ± 3.4% in G3. Bands at 10–35 kDa were not detected in G3, and the relative intensity of bands above 200 kDa decreased from 22.1 ± 2.6% in G1 to 11.2 ± 0.8% in G3. The SDS-PAGE findings provide orthogonal, albeit non-specific, evidence of enrichment, indicating a cleaner electrophoretic profile. However, by themselves, they do not validate the FTIR spectral features as indicators of purity and do not replace direct protein identification or determination of absolute protein purity.

FTIR spectroscopy may ultimately provide a rapid in-process fingerprinting tool for this manufacturing workflow. Before routine implementation, the method requires harmonized sample preparation, a larger and statistically justified set of independent batches, predefined acceptance criteria, external validation, and comparison with orthogonal identity, purity, aggregation, and functional assays.

Any future implementation of FTIR as a routine in-process control must be based on a harmonized sampling protocol, and the spectral fingerprints must be validated against independent reference methods.

Acknowledgments

The authors thank the institutions and colleagues who supported preparation of this manuscript. A.A. Surkova acknowledges financial support from the ITMO Fellowship Program.

Conflicts of interest: Authors declare no conflicts of interest.

Funding: This study was funded by the Ministry of Health of the Russian Federation under the state assignment for the research and development project “Development of human donor blood-derived bioproducts for regenerative personalized medicine and three-dimensional bioprinting.”

Data availability: Data supporting the findings are included in the article and its Supplementary Information. Raw FTIR spectra and gel images are available from the corresponding author upon reasonable request, subject to institutional data-sharing requirements.

Artificial intelligence (AI) use statement: No generative AI was used for data collection, experimental design, statistical analysis, or interpretation of results.

Submitted: 01 August 2026
Accepted: 18 September 2026
Published online: 06 October 2026

References

[1] Volkova LV, Shultz EV. Perspektivy ispolzovaniya pobochnykh produktov fraktsionirovaniya donorskoy plazmy [Potential applications of by-products of donor plasma fractionation]. Vestn PNIPU Khim Tekhnol Biotekhnol 2015;(4). Russian. Available from: https://cyberleninka.ru/article/n/perspektivy-ispolzovaniya-pobochnyh-produktov-fraktsionirovaniya-donorskoy-plazmy. Accessed June 16, 2026.

[2] Cohn EJ, Strong LE, Hughes WL, et al. Preparation and properties of serum and plasma proteins. IV. A system for the separation into fractions of the protein and lipoprotein components of biological tissues and fluids. J Am Chem Soc 1946;68(3):459–75. https://doi.org/10.1021/ja01207a034

[3] Sierra-Sánchez Á, Sanabria-de la Torre R, Ubago-Rodríguez A, et al. Blood plasma, fibrinogen or fibrin biomaterial for the manufacturing of skin tissue engineered products and other dermatological treatments: a systematic review. J Funct Biomater 2025;16(3):79. https://doi.org/10.3390/jfb16030079

[4] Pankov R, Yamada KM. Fibronectin at a glance. J Cell Sci 2002;115(20):3861–3. https://doi.org/10.1242/jcs.00059

[5] Son B, Kim M, Won H, et al. Secured delivery of basic fibroblast growth factor using human serum albumin based protein nanoparticles for enhanced wound healing and regeneration. J Nanobiotechnology 2023;21:310. https://doi.org/10.1186/s12951-023-02053-4

[6] Kliuchnikova AA, Novikova SE, Ilgisonis EV, et al. Blood plasma proteome: a meta-analysis of the results of protein quantification in human blood by targeted mass spectrometry. Int J Mol Sci 2023;24(1):769. https://doi.org/10.3390/ijms24010769

[7] Risman RA, Sen M, Tutwiler V, Hudson NE. Deconstructing fibrin(ogen) structure. J Thromb Haemost 2025;23(2):368–80. https://doi.org/10.1016/j.jtha.2024.10.024

[8] Ryabov NA, Karyakina OA, Volova LT. Sposob polucheniya fibrinogensoderzhashchego kompaunda na osnove pobochnogo produkta fraktsionirovaniya donorskoy plazmy cheloveka [Method for obtaining a fibrinogen-containing preparation from a by-product of human donor-plasma fractionation]. Russian patent application No. 2026121604. Filed July 6, 2026. Applicant: Samara State Medical University.

[9] Usoltsev D, Sitnikova V, Kajava A, Uspenskaya M. Systematic FTIR spectroscopy study of the secondary structure changes in human serum albumin under various denaturation conditions. Biomolecules 2019;9(8):359. https://doi.org/10.3390/biom9080359

[10] Massei A, Falco N, Fissore D. Use of Raman spectroscopy and PCA for quality evaluation and out of specification identification in biopharmaceutical products. Eur J Pharm Biopharm 2024;201:114342. https://doi.org/10.1016/j.ejpb.2024.114342

[11] Wang H, Ding X, He X, et al. Application of ATR-FTIR spectroscopy and chemometrics for the forensic discrimination of aged peripheral and menstrual bloodstains. Microchem J 2024;197:109933. https://doi.org/10.1016/j.microc.2024.109933

[12] Sandt C. Identification and classification of proteins by FTIR microspectroscopy. A proof of concept. Biochim Biophys Acta Gen Subj 2024;1868(10):130688. https://doi.org/10.1016/j.bbagen.2024.130688

[13] Delbeck S, Heise HM. Systematic stability testing of insulins as representative biopharmaceuticals using ATR FTIR spectroscopy with focus on quality assurance. J Biomed Opt 2021;26(4):043007. https://doi.org/10.1117/1.JBO.26.4.043007

[14] van de Weert M, Haris PI, Hennink WE, Crommelin DJA. Fourier transform infrared spectrometric analysis of protein conformation: effect of sampling method and stress factors. Anal Biochem 2001;297(2):160–9. https://doi.org/10.1006/abio.2001.5337

[15] Litvinov RI, Faizullin DA, Zuev YF, Weisel JW. The α helix to β sheet transition in stretched and compressed hydrated fibrin clots. Biophys J 2012;103(5):1020–7. https://doi.org/10.1016/j.bpj.2012.07.046

[16] Sachdeva A, Cai S. Structural differences of proteins between solution state and solid state probed by attenuated total reflection Fourier transform infrared spectroscopy. Appl Spectrosc 2009;63(4):458–64. https://doi.org/10.1366/000370209787944316

[17] Laemmli UK. Cleavage of structural proteins during the assembly of the head of bacteriophage T4. Nature 1970;227(5259):680–5. https://doi.org/10.1038/227680a0

[18] Jolliffe IT. Principal component analysis. 2nd ed. New York: Springer; 2002. 487 p. (Springer Series in Statistics). https://doi.org/10.1007/b98835

[19] Yang S, Zhang Q, Yang H, et al. Progress in infrared spectroscopy as an efficient tool for predicting protein secondary structure. Int J Biol Macromol 2022;206:175–87. https://doi.org/10.1016/j.ijbiomac.2022.02.104

[20] Wolberg AS, Campbell RA. Fibrinogen and fibrin: synthesis, structure, and function in health and disease. J Thromb Haemost 2023;21(11):3005–15. https://doi.org/10.1016/j.jtha.2023.08.014

[21] Brennan SO. Electrospray ionisation analysis of human fibrinogen. Thromb Haemost 1997;78(3):1055–8. https://doi.org/10.1055/s-0038-1657686
[22] Matsuka YV, Migliorini MM, Ingham KC. Cross-linking of fibronectin to C-terminal fragments of the fibrinogen alpha chain by factor XIIIa. J Protein Chem 1997;16(8):739–45. https://doi.org/10.1023/A:1026307731751
[23] Fu Y, Grieninger G. FIB(420):a normal human variant of fibrinogen with two extended alpha chains. Proc Natl Acad Sci USA 1994;91(7):2625–8. https://doi.org/10.1073/pnas.91.7.2625
[24] Weinstein MJ, Deykin D. Quantitative abnormality of an Aα chain molecular weight form in the fibrinogen of cirrhotic patients. Br J Haematol 1978;40(4):617–30. https://doi.org/10.1111/j.1365-2141.1978.tb05838.x
[25] Weinstein MJ, Deykin D. The A alpha chain composition of low-solubility fibrinogen. Thromb Res 1980;17(1–2):281–3. https://doi.org/10.1016/0049-3848(80)90315-1
[26] Weisel JW, Litvinov RI. Fibrin formation, structure and properties. In: Parry DAD, Squire JM, editors. Fibrous proteins: structures and mechanisms. Cham: Springer International Publishing; 2017. p. 405–56. (Subcellular Biochemistry; vol. 82).https://doi.org/10.1007/978-3-319-49674-0_13
[27] Mosesson MW. Fibrinogen and fibrin structure and functions. J Thromb Haemost 2005;3(8):1894–904. https://doi.org/10.1111/j.1538-7836.2005.01365.x
[28] Klaubert W, Schulte Derne O, Gollwitzer R, et al. Limited fibrinogenolysis in stored whole blood and in fresh frozen plasma. Thromb Res 1988;50(1):43–51. https://doi.org/10.1016/0049-3848(88)90173-9
[29] Lau HK. Anticoagulant function of a 24 Kd fragment isolated from human fibrinogen A alpha chains. Blood 1993;81(12):3277–84. https://doi.org/10.1182/blood.V81.12.3277.bloodjournal81123277
[30] McKee PA, Mattock P, Hill RL. Subunit structure of human fibrinogen, soluble fibrin, and cross-linked insoluble fibrin. Proc Natl Acad Sci USA 1970;66(3):738–44. https://doi.org/10.1073/pnas.66.3.738
[31] De Meutter J, Goormaghtigh E. Amino acid side-chain contribution to protein FTIR spectra: impact on secondary-structure evaluation. Eur Biophys J 2021;50(3–4):641–51. https://doi.org/10.1007/s00249-021-01507-7
[32] Goormaghtigh E, Cabiaux V, Ruysschaert JM. Secondary structure determination of proteins in aqueous solution by attenuated total-reflection FT-IR. Eur J Biochem 1990;193(2):409–20. https://doi.org/10.1111/j.1432-1033.1990.tb19354.x
[33] Guo S, Rösch P, Popp J, Bocklitz T. Modified PCA and PLS: toward better classification in Raman spectroscopy-based biological applications. J Chemom 2020;34(5):e3202. https://doi.org/10.1002/cem.3202
[34] Lomont JP, Rich KL, Maj M, et al. A spectroscopic signature for stable β-amyloid fibrils versus β-sheet-rich oligomers. J Phys Chem B 2018;122(1):144–53. https://doi.org/10.1021/acs.jpcb.7b10765
[35] Olesen PR, Sorensen MS, Nielsen JR, et al. Effects of potassium bromide disk formation on the infrared spectra of dried model proteins. J Pharm Sci 2004;93(2):496–506. https://doi.org/10.1002/jps.10563
[36] Militello V, Casarino C, Emanuele A, et al. Aggregation kinetics of bovine serum albumin studied by FTIR spectroscopy and light scattering. Biophys Chem 2004;107(2):175–87. https://doi.org/10.1016/j.bpc.2003.09.004
[37] Burnouf T. Modern plasma fractionation. Transfus Med Rev 2007;21(2):101–17. https://doi.org/10.1016/j.tmrv.2006.11.001
[38] Pieters M, Wolberg AS. Fibrinogen and fibrin: an illustrated review. Res Pract Thromb Haemost 2019;3(2):161–72. https://doi.org/10.1002/rth2.12191
[39] Lanir N, Ciano PS, Van de Water L, et al. Macrophage migration in fibrin gel matrices. II. Effects of clotting factor XIII, fibronectin, and glycosaminoglycan content on cell migration. J Immunol 1988;140(7):2340–9. https://doi.org/10.4049/jimmunol.140.7.2340

Related article

1. Analysis of pulmonary surfactant by Fourier transform infrared spectroscopy after exposure to sevoflurane and isoflurane

Vilena Vrbanović Mijatović et al., BJBMS, 2017